Extended data Figure 1

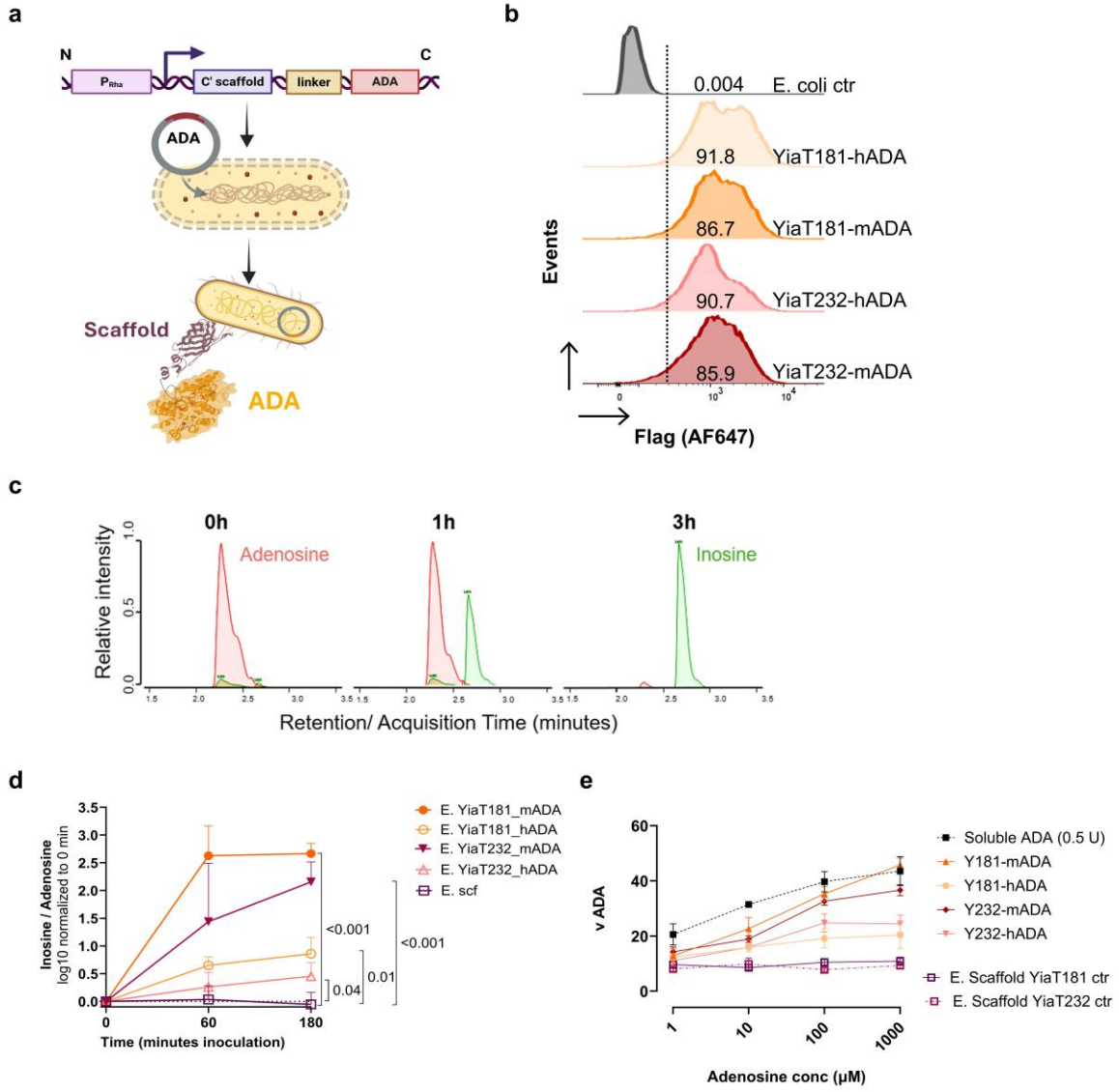

Extended Data Fig. 1: Surface display and enzymatic activity of human and murine ADA. **a,** Bacterial surface-display strategy comprising the expression plasmid, scaffold–GS linker–ADA1 fusion and surface presentation in *E. coli* DH5α. Protein structures were predicted using AlphaFold v.2 and visualized in PyMOL. Created with BioRender.com. **b,** Representative histograms of surface-exposed FLAG-tagged scaffold YiaT181 and YiaT232 displaying murine ADA (mADA) or human ADA (hADA), with FLAG-negative bacteria control. **c,** Representative LC–MS chromatograms of adenosine (ADO, red) depletion and inosine (INO, green) formation during incubation with ADA-displaying *E. coli* (YiaT181-murine ADA). **d,** INO/ADO ratio at 0, 60 and 180 min for hADA and mADA displayed by YiaT181 or YiaT232, with E. scf control. **e,** Reaction velocity across increasing ADO concentrations for YiaT181- and YiaT232-displayed hADA and mADA, with the corresponding scaffold controls. Soluble ADA (0.5 U per reaction; Roche) served as a positive control. Mean±s.e.m.; *n*=3 (**d**) and *n*=4 (**e**) biological replicates from two independent

experiments. **d,** Two-way ANOVA with Holm–Šídák's test. **e,** Vmax and Km estimates with 95% confidence intervals are provided in Supplementary Table S3.

Extended data Figure 2

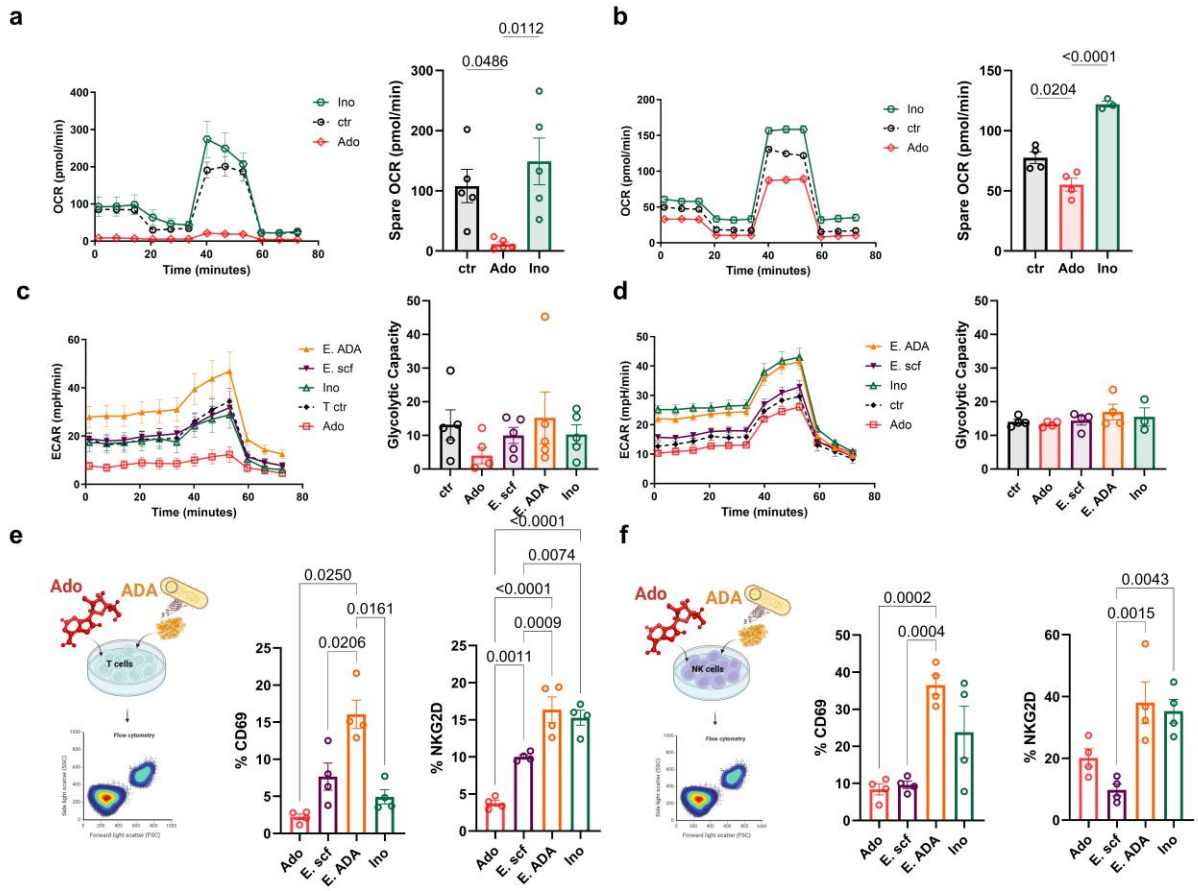

Extended Data Fig. 2. ADA restores immune-cell metabolic and activation-associated phenotypes under adenosine stress. a,**b,** Oxygen consumption rate (OCR) profiles and quantification of spare respiratory capacity in primary human T (**a**) and NK cells (**b**) exposed to adenosine (ADO), inosine (INO) or DMSO control. **c,d,** Extracellular acidification rate (ECAR) profiles and corresponding glycolytic-function measurements in T cells (**c**) and NK cells (**d**) following treatment with ADO alone or with scaffold-control (*E.* scf) or ADA-displaying bacteria (*E.* ADA), with INO and untreated cells included as indicated. **e,f,** Flow-cytometric analysis of activation-associated surface markers in ADO-stressed T cells (**e**; CD69 and NKG2D) and NK cells (**f**; NKG2D and CD25) following exposure to E. scf or *E.* ADA. Mean±s.e.m. of n=5 (**a**,**c**) and n=4 (**b,d**,**e,f**) biological replicates and independent donors. Individual points represent independent donors. (**a**-**f**) One-way ANOVA with Tukey's post-hoc test.

Extended data Figure 3

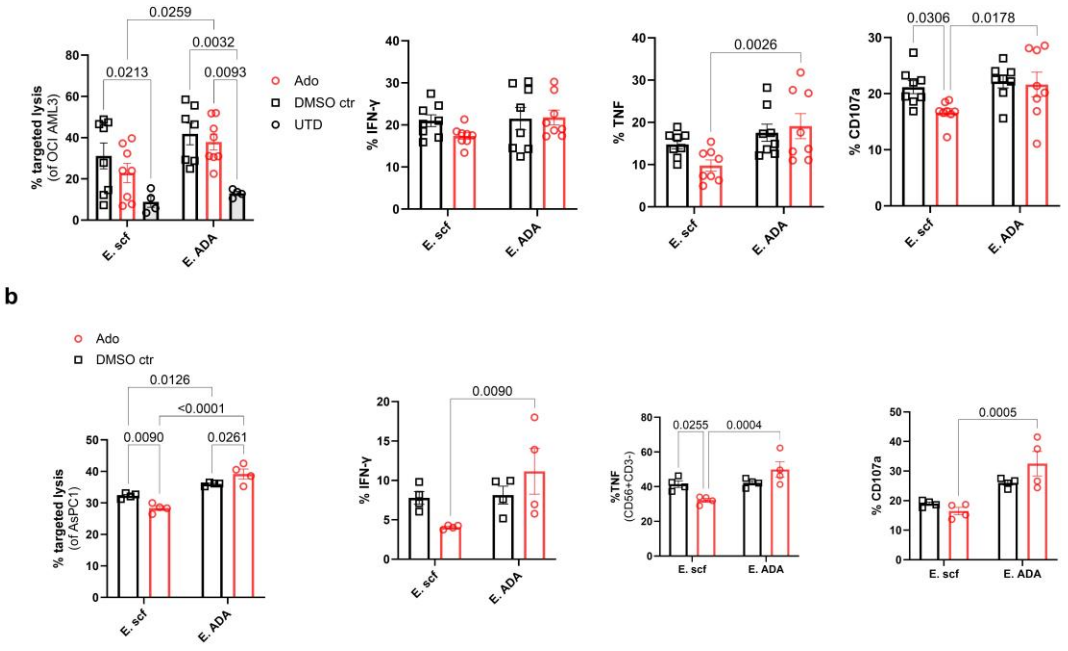

Extended Data Fig. 3. ADA-mediated metabolic rescue restores cytotoxicity in NK and CAR-T cells. a,b, Cytotoxic activity of **(a)** NK cells against human AsPC1 pancreatic ductal adenocarcinoma (PDAC) cells and **(b)** CD70 CAR-T cells against human OCI-AML3 acute myeloid leukemia (AML) cells following exposure to scaffold control (E. scf) or ADA-displaying bacteria (E. ADA) under adenosine (ADO)-supplemented or DMSO control conditions. Cytotoxic activity was assessed by target cell lysis, intracellular IFN-γ and TNF expression, and surface CD107a expression. Untransduced T cells (UTD) served as a CAR-negative effector-cell control for targeted lysis experiments. Cytotoxicity was assessed after **a,** 16h and **b,** 24 to 36h at an effector-to-target (E:T) ratio of 1:1. Mean±s.e.m. of n=4 (**a**) and n=8 (**b**) biologically independent donor derived effector cells. Two-way ANOVA.

Extended data Figure 4

a

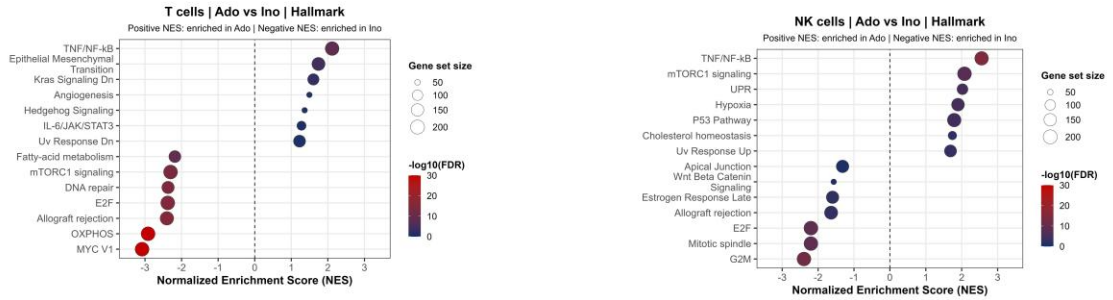

b

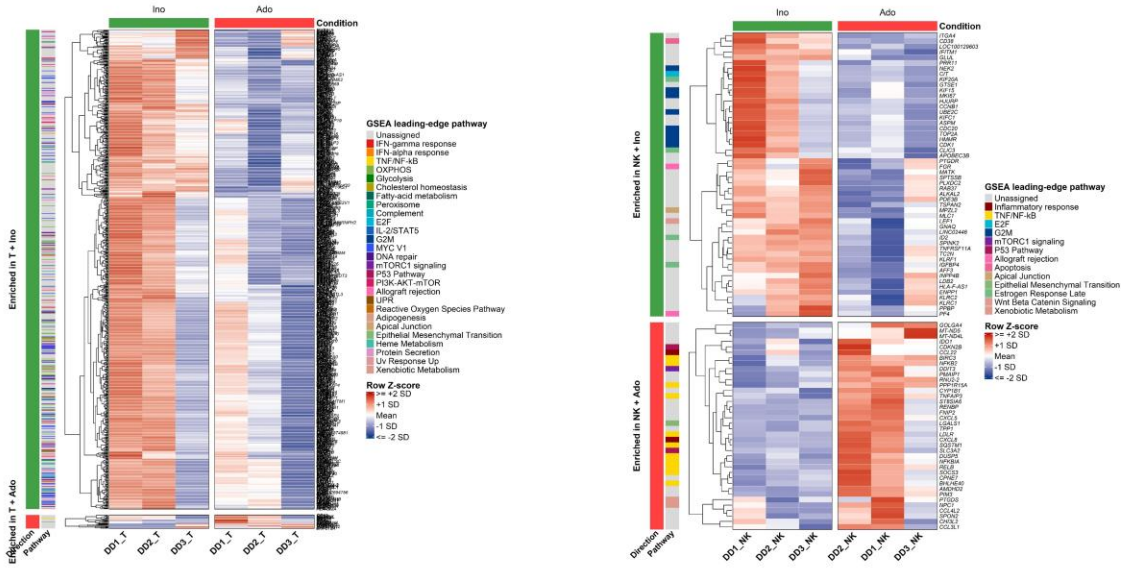

Extended Data Fig. 4. INO shifts human T and NK cells towards metabolic and proliferative transcriptional programs. a, Gene set enrichment analysis (GSEA) of MSigDB Hallmark pathways in primary human T cells (left) and NK cells (right) from three donors exposed to ADO (red) or INO (green). Positive normalized enrichment scores (NES) indicate enrichment in ADO-exposed cells and negative NES enrichment in INO-exposed cells. Dot size indicates gene-set size and color indicates −log10 false-discovery rate (FDR). **b,** Pathway-independent heatmaps of differentially expressed genes in NK cells (left) and T cells (right) from three donors exposed to ADO versus INO. Differentially expressed genes were identified independently of pathway membership, separated according to the direction of differential expression and hierarchically clustered within each direction. Columns represent individual donors and colors indicate gene-wise z-scores of variance-stabilized expression, truncated at ±2. Side annotations indicate subsequent membership in selected Hallmark GSEA leading-edge gene sets; genes not represented in the displayed leading edges are labelled unassigned. GSEA pathway membership did not influence gene selection or clustering. Differential expressions were analyzed using DESeq2 with donor included in the model. ADO, adenosine; FDR, false-discovery rate; GSEA, gene set enrichment analysis; INO, inosine; NES, normalized enrichment score.

Extended data Figure 5

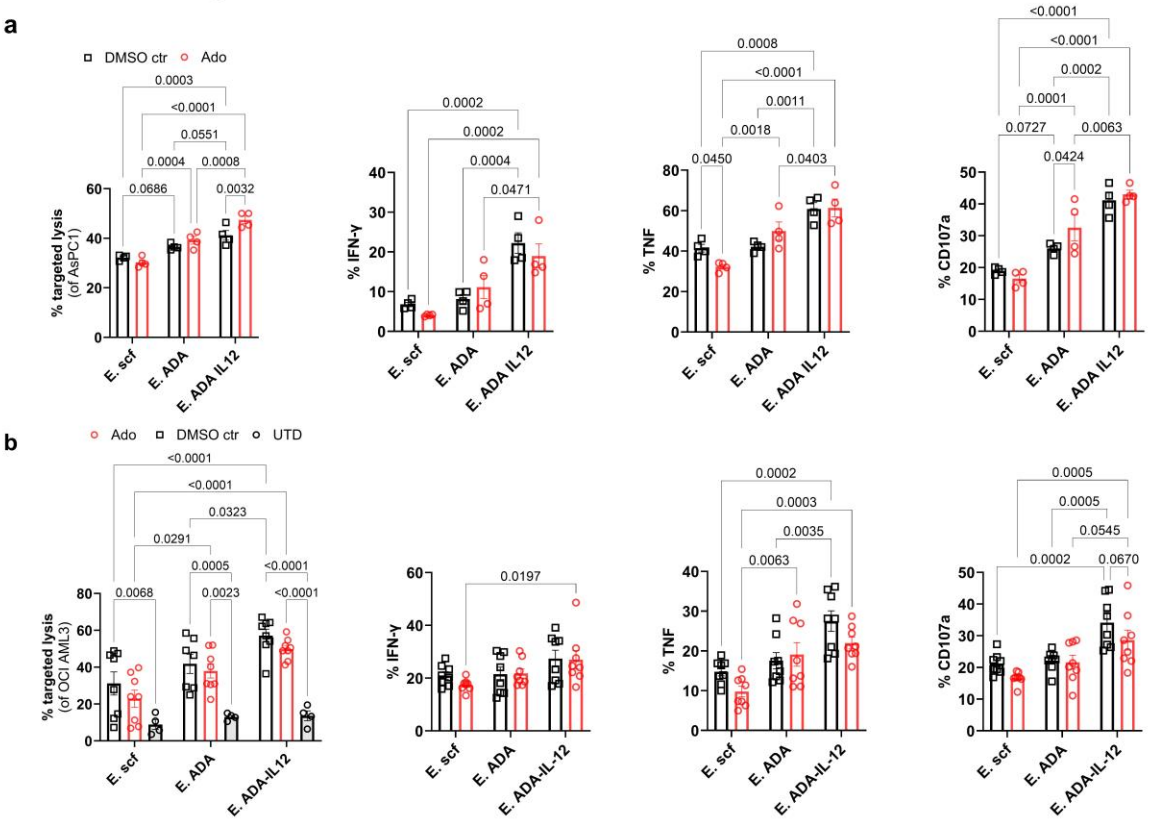

Extended Data Fig. 5. ADA–IL-12 enhances NK- and CD70 CAR-T-cell cytotoxic and effector function under adenosine stress. a,b, Effector-cell cytotoxicity and associated cytokine production and degranulation following exposure to scaffold-control bacteria (E. scf), ADA-displaying bacteria (E. ADA) or dual ADA–IL-12-displaying bacteria (E. ADA–IL-12), in the presence or absence of adenosine (ADO). **a,** NK-cell-mediated cytotoxicity against human AsPC1 pancreatic cancer cells after 24–36 hours, with intracellular TNF and IFN-γ production and surface CD107a expression in NK-cell effectors (n=4 biologically independent donor-derived NK-cell samples). **b,** CD70 CAR-T-cell-mediated cytotoxicity against human OCI-AML3 acute myeloid leukemia (AML) cells after 16 hours, with intracellular IFN-γ and TNF production and surface CD107a expression in CAR-T-cell effectors (n=8 biologically independent donor-derived CAR-T-cell samples). Untransduced T cells (UTD) served as CAR-negative effector-cell controls for the cytotoxicity assay. All cytotoxicity assays were performed at an effector-to-target (E:T) ratio of 1:1. Mean±s.e.m.; individual points represent biologically independent donor-derived effector-cell samples. Two-way ANOVA with Tukey's multiple-comparisons test.

Extended Data Figure 6

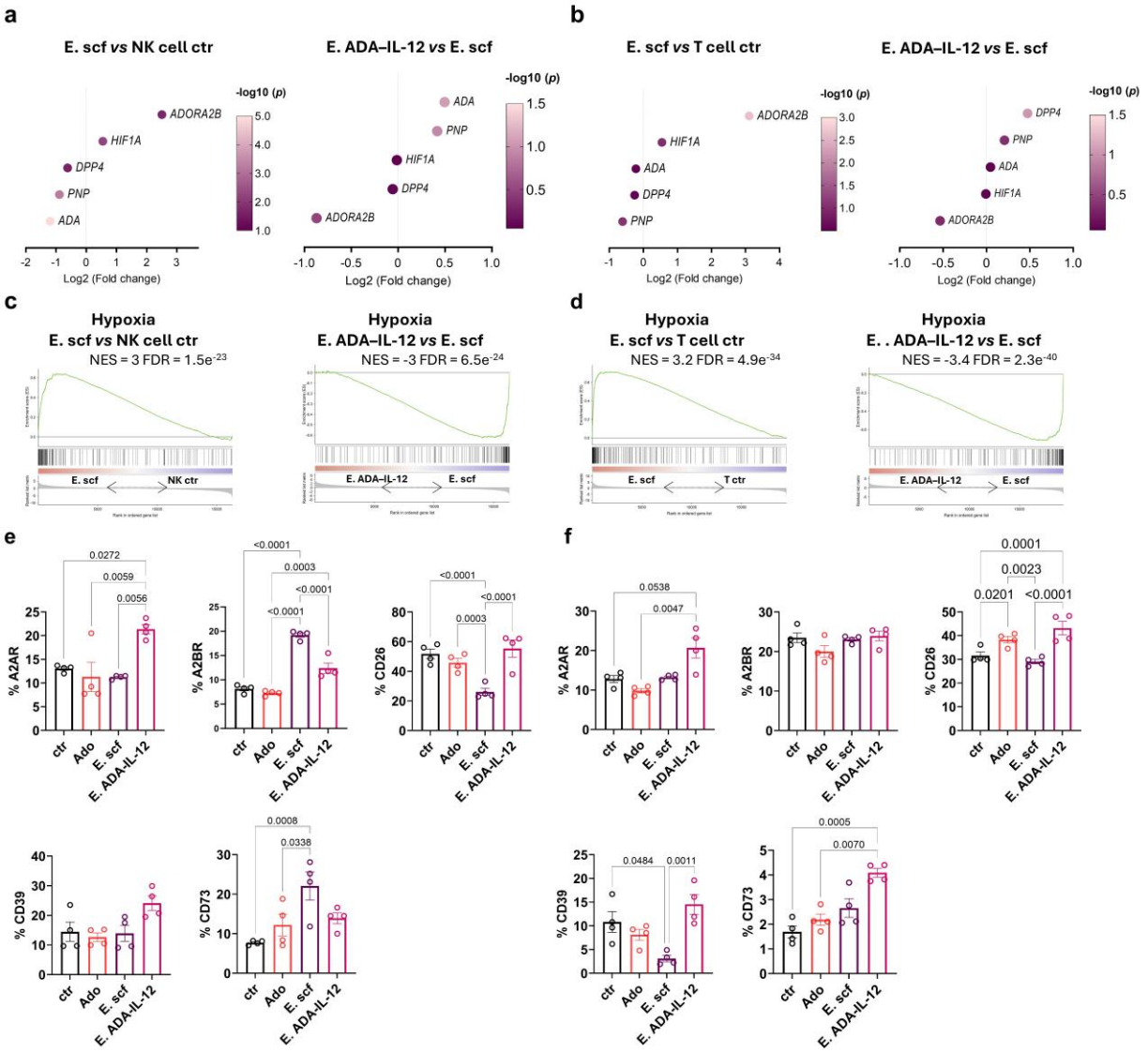

Extended Data Fig. 6. Remodeled Adenosine-signaling in human NK and T cells. a,b, Differential expression of selected adenosine-, purine metabolism- and hypoxia-associated genes in **a,** primary human NK cells and **b,** T cells exposed to E. scf or E. ADA–IL-12. Color indicates −log10 FDR-adjusted *P* value; dashed line, log2FC = 0. Differential expression was assessed using DESeq2 with the Wald test and Benjamini–Hochberg correction. **c,d,** GSEA enrichment profiles of the MSigDB Hallmark Hypoxia gene set in **c,** NK cells and **d,** T cells comparing ctr with E. scf and E. scf with E. ADA–IL-12. NES and FDR are shown. **a–d,** n=3 biologically independent donors. **e,f,** Flow-cytometric analysis of A2AR (*ADORA2A*), A2BR (*ADORA2B*), CD26 (*DPP4*), CD39 (*ENTPD1*), and CD73 (*NT5E*) surface expression in **e,** NK cells and **f,** T cells exposed to ctr, ADO, E. scf or E. ADA–IL-12. Mean±s.e.m.; n=4 biologically independent donors. Statistical significance was assessed by one-way ANOVA followed by Tukey's multiple-comparisons test.

Extended data Figure 7

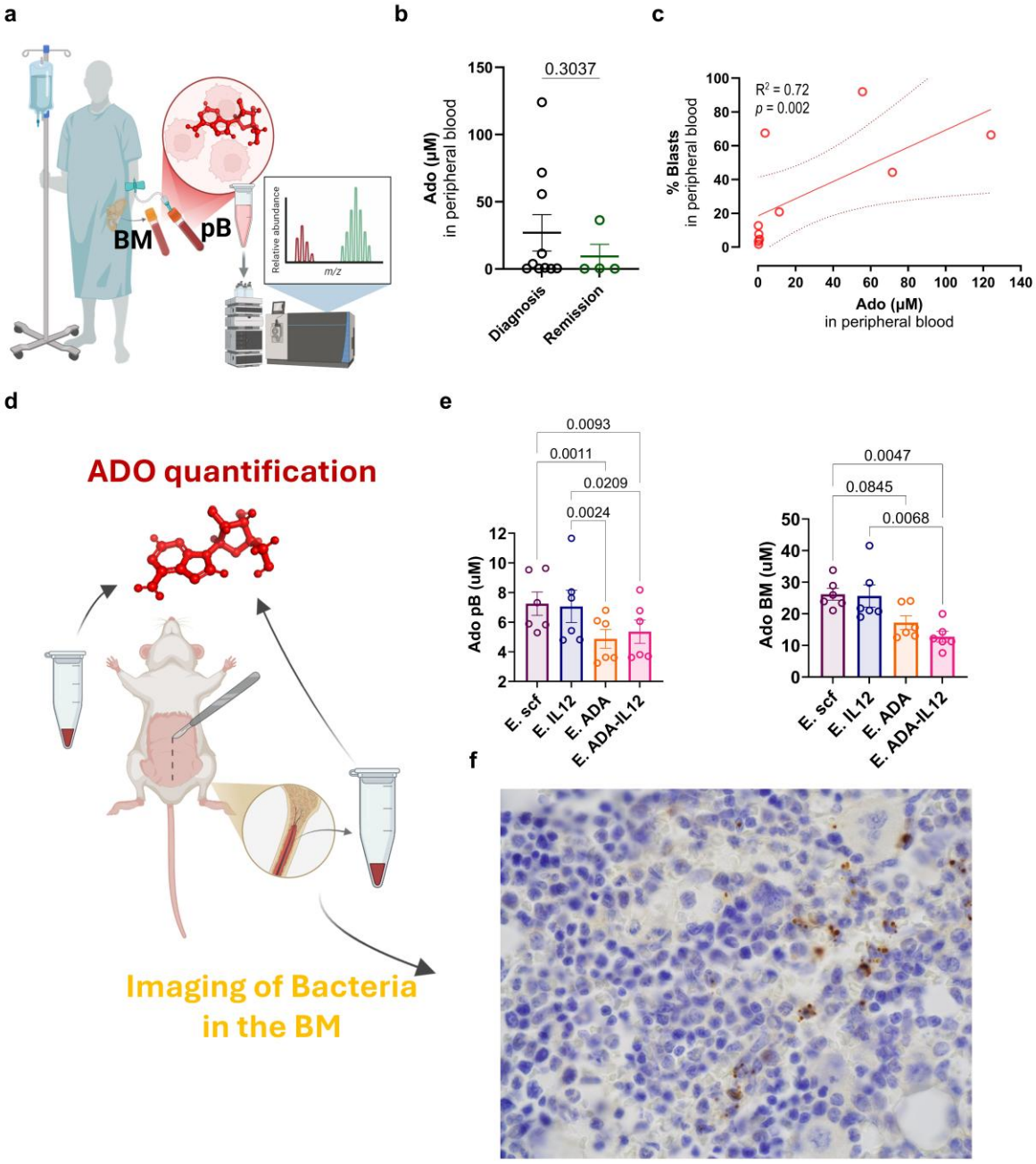

Extended Data Fig. 7. Adenosine levels are associated with leukemic burden and are reduced by bacteria-displayed ADA in AML. a, Analysis schema of plasma adenosine (ADO) and leukemic blast burden in patient-derived peripheral blood (PB) and bone marrow (BM). Created with BioRender.com. **b,** Plasma ADO concentrations in PB from patients with AML at diagnosis and remission. **c,** Correlation between PB plasma ADO concentrations and circulating blast percentage at diagnosis. Solid line, linear regression; dashed lines, 95% confidence interval. **d,** WEHI-3B AML analysis schema. PB and BM were collected 2 hours after the second bacterial administration on day 10 for ADO quantification and BM bacterial localization. Created with

BioRender.com. **e,** ADO concentrations in PB and BM of WEHI-3B-bearing mice treated with PBS, E. scf, E. IL-12, E. ADA or E. ADA–IL-12 assessed on day 14. **f,** Representative BM section 2 hours after the second bacterial administration showing phagocytosed *E. Coli* (E. scf) bacterial rods (in brown) within neutrophilic granulocytes, highlighted by immunohistochemical stain using antibody against E. coli O/K with HRP/DAB detection and hematoxylin counterstaining. Image was acquired at ×1,000 magnification using an Olympus BX46 microscope equipped with a DP27 camera. Mean±s.e.m. (**b,e**); symbols represent biological samples. **b,** Two-sided Mann–Whitney U-test; **c,** Pearson correlation; **e,** one-way ANOVA with Tukey's multiple comparison test.

Extended data Figure 8

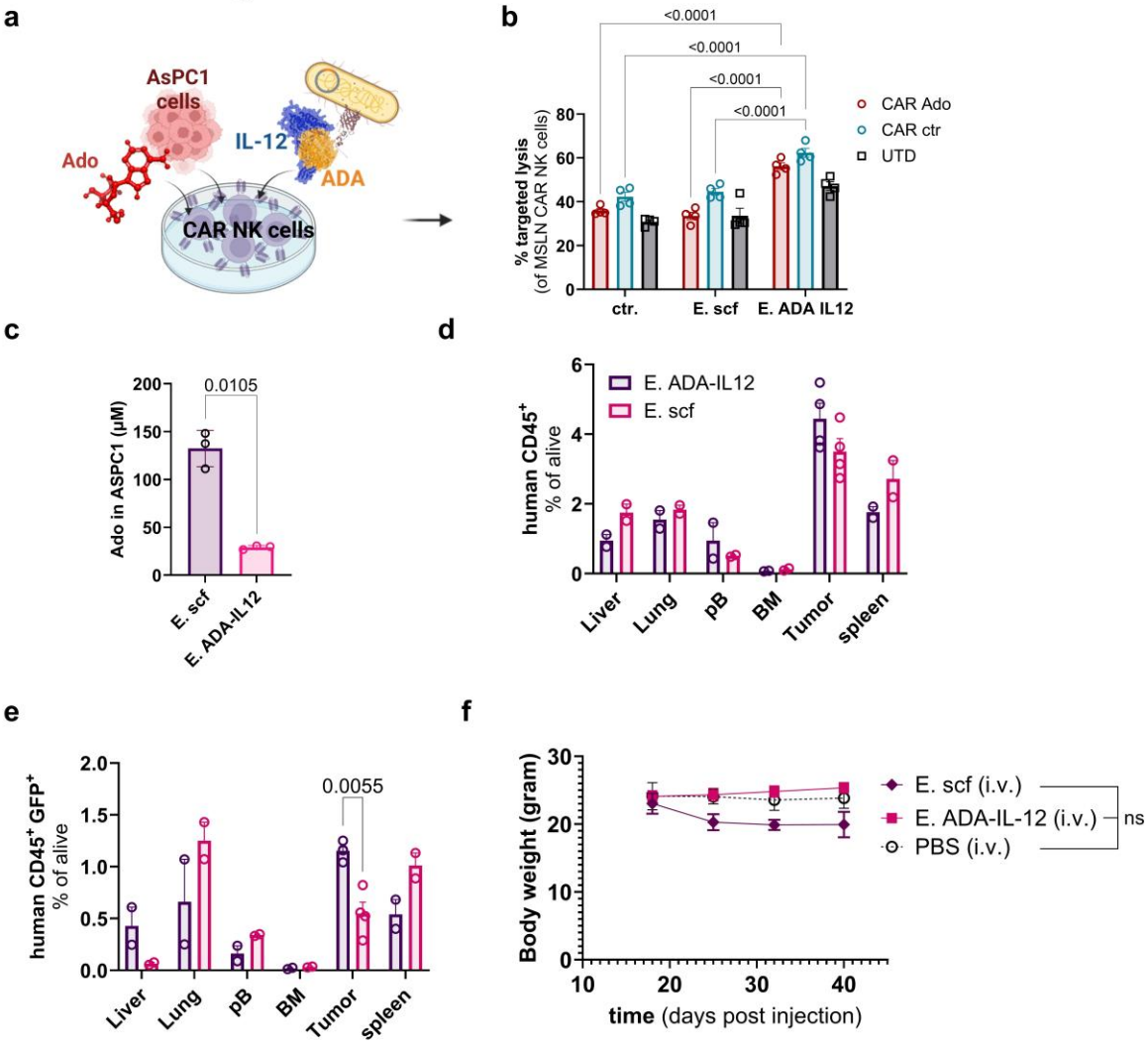

Extended Data Fig. 8: E. ADA–IL-12 enhances MSLN CAR-NK-cell cytotoxicity and supports CAR-NK-cell accumulation in AsPC1 xenografts. a, Schematic of MSLN CAR-NK-cell cytotoxicity assays against human AsPC1 pancreatic cancer cells under adenosine (ADO) exposure and treatment with the indicated bacterial constructs. **b,** Cytotoxicity of MSLN CAR-NK cells (n=4) against AsPC1 target cells at a 1:1 effector-to-target (E:T) ratio following treatment with the indicated *E. coli* constructs in the presence of ADO or DMSO control (ctr.). Untransduced NK cells (UTD) served as a CAR-negative control. Target-cell lysis was quantified relative to target-only controls. **C**, ADO levels in AsPC1 tumors of E. ADA–IL-12 and E. scf treated mice (n=3). **d,** Frequencies of human CD45$^+$ (huCD45$^+$) cells and **e**, human CD45$^+$ and GFP$^+$ cells among viable cells in bone marrow (BM), liver, lung, peripheral blood (PB), tumor and spleen on day 36 following treatment with MSLN CAR NK cells with E. ADA–IL-12, E. scf and PBS of n=4 different tumors from two mice. **f,** Body-weight in mice bearing AsPC1 pancreatic cancer cells following treatment MSLN CAR NK with PBS n=3, scaffold-control bacteria (E. scf, n=6), or dual

ADA–IL-12-displaying bacteria (E. ADA–IL-12, n=7). Mean ± s.e.m.; One-way ANOVA with Tukey's multiple comparison test.